AGU PUBLICATIONS

Water Resources Research

RESEARCH ARTICLE
10.1002/2016WR018915

Instability of canopy flows

Giuseppe A. Zampogna[1], Franck Pluvinage[2], Azeddine Kourta[2], and Alessandro Bottaro[1]

[1]Department of Civil, Chemical and Environmental Engineering, University of Genova, Italy, [2]Université d'Orléans, INSA-CVL, PRISME EA4229, Orléans, France

Key Points:
- New stability theory of flows over canopies
- Comparison of two different methods with experiments
- Advantage of the new method over classical approaches (based on a scalar drag coefficient)

Correspondence to:
A. Bottaro,
alessandro.bottaro@unige.it

Citation:
Zampogna, G. A., F. Pluvinage, A. Kourta, and A. Bottaro (2016), Instability of canopy flows, *Water Resour. Res.*, *52*, 5421–5432, doi:10.1002/2016WR018915.

Received 16 MAR 2016
Accepted 20 JUN 2016
Accepted article online 22 JUN 2016
Published online 16 JUL 2016

Abstract *Honami* and *monami* waves are caused by large-scale coherent vortex structures which form in shear layers generated by canopies. In order to reach new insights on the onset of such waves, the instability of these shear layers is studied. Two different approaches are used. In the first approach, the presence of the canopy is modeled via a drag coefficient, taken to vary along the canopy as by experimental indications. The second approach considers the canopy as a porous medium and different governing equations for the fluid flow are deduced. In this second case, the anisotropy of the canopy, composed by rigid cylindrical elements, is accounted for via an *apparent* permeability tensor. The results obtained with the latter approach approximate better experimental correlations for the synchronous oscillations of the canopy.

1. Introduction

Flow-induced plant motion in atmospheric or aquatic boundary layers has recently been object of much interest [*Nepf*, 1999; *Finnigan*, 2000; *De Langre*, 2008; *Battiato and Rubol*, 2014; *le Bouteiller and Venditti*, 2015], because of its influence on plant growth, transport of sediments, pollens, contaminants, or biomass production.

When fluid moves above and through plants, the drag force associated with the presence of the vegetation causes an inflection point in the mean velocity profile. This, in turn, might be responsible for the occurrence of a Kelvin-Helmholtz instability which initiates the formation of large-scale coherent flow structures above the canopy. Such large-scale waves are associated to a synchronous waving of the canopy, called *monami* for the case of sea grass beds and *honami* for terrestrial crops. Thus, the presence of a shear layer near the top of the vegetation bed, and its instability, have been related, since the study by *Raupach et al.* [1996], to the onset of large-scale, coherent oscillations of the plants.

Although the canopy is frequently modeled in the laboratory by using flexible elements hinged at the wall [*Meroney*, 1968; *Novak et al.*, 2002; *Farquhar et al.*, 2003; *Doaré et al.*, 2004], experiments [*Ghisalberti and Nepf*, 2002, 2004, 2005] have demonstrated that the shear layer instability persists when rigid dowels are used instead; this is why we assume in the following that grass blades are rigid and oriented orthogonally to the surface. In the past, mean velocity profiles of the shear layer have been taken to be either piecewise linear [*Py et al.*, 2004; *Doaré et al.*, 2004] or in the shape of hyperbolic tangent profiles [*Ghisalberti and Nepf*, 2002; *Raupach et al.*, 1996]. These represent coarse approximations of the experimentally measured profiles [*Ghisalberti and Nepf*, 2004]. A different approach to infer mean flow profiles and to write perturbation equations has been pursued by *Singh et al.* [2015], through the use of momentum balance equations, with account of the drag force through the canopy.

In this work, the linear stability analysis of canopy flows will be performed. We have chosen to model the steady mean flow through the rigid canopy as accurately as possible, by employing a method initiated by *Ghisalberti and Nepf* [2004], to treat four scenarios from the literature [*Ghisalberti and Nepf*, 2002, 2004, 2005]. In the following, we call this approach **A**. A second approach (**B**) pursued here consists in considering the flow in the canopy as the motion through a dense porous medium ruled by Darcy's equation. This second approach to describe the mean flow through a orthotropic medium is thoroughly described and validated by *Zampogna and Bottaro* [2016] and is summarized in the Appendix A.

Linear stability equations are written for both approaches, and solved both without and with drag through the canopy, demonstrating that canopy drag reduces the growth rate of the shear layer instability, in

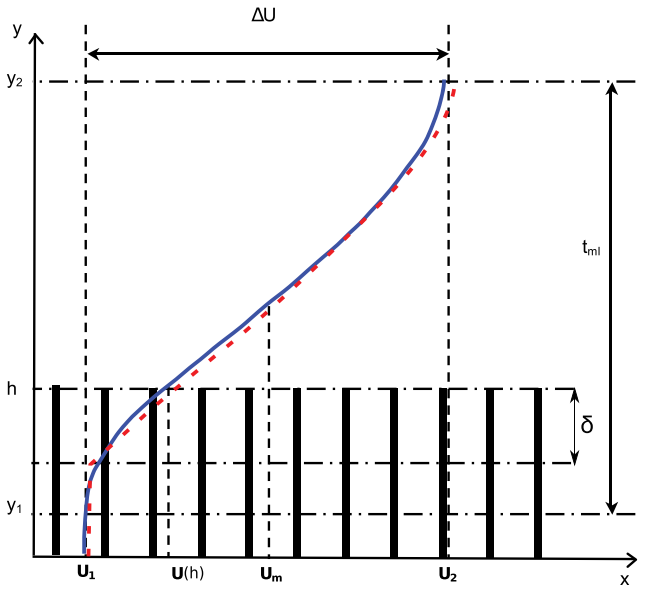

Figure 1. Mean flow velocity profile through a rigid canopy computed with method **A** and **B** (solid blue and dashed red curves, respectively).

agreement with previous studies [*Py et al.*, 2004, 2006]. Wavelengths and frequencies of the most unstable modes are computed for the two approaches, and compared with one another and with experimental correlations available from the literature. The second approach, which couples Rayleigh equation in the nonvegetated zone to Darcy's equation through the vegetation, provides more reliable results, probably because of the account of anisotropic features in the canopy layer.

2. The Mean Flow: The Drag Coefficient Approach Versus Euler-Darcy Coupling

The mean velocity of the fluid through and outside the canopy is sketched in Figure 1. A mixing layer develops, because of canopy drag, and its thickness is denoted by t_{ml}; the velocity profile ranges between two extreme values, one, U_1, which is found in the region from the channel bottom at $y = 0$ to $y = y_1$ (the bottom, influential boundary layer is neglected), and the other, U_2, which prevails for $y > y_2$ ($y_2 - y_1 = t_{ml}$). The mean velocity is $U_m = (U_1 + U_2)/2$. The height of the canopy is denoted by h; the height of the flow channel of the experiments by *Ghisalberti and Nepf* [2004, 2005] is equal to 3.38 h. In the present analysis, the air-water interface is not modeled and an indefinitely high water channel is considered. While this differs from the experimental conditions, we do not expect free surface waves to hold a significant role in the onset of the instabilities observed near the canopy's edge. This is supported by *Brevis et al.* [2014] where it is shown that, for very low Froude numbers, such as in the present case, water surface fluctuations are negligible.

As stated earlier, two approaches will be pursued, both in modelling the mean flow and in establishing the disturbance equations; they will be denoted approach **A** and **B**.

Using the Reynolds' decomposition for the instantaneous velocity and pressure, $u_i = U_i + u_i'$, $p = P + p'$, for the incompressible motion of a constant density (ρ) fluid, and averaging (this operation is indicated by overbars), we have:

$$\frac{\partial U_i}{\partial x_i} = 0, \tag{1}$$

$$\rho\left(\frac{\partial U_i}{\partial t} + U_j\frac{\partial U_i}{\partial x_j} + \overline{u'_j\frac{\partial u'_i}{\partial x_j}}\right) = -\frac{\partial P}{\partial x_i} + \mu\frac{\partial^2 U_i}{\partial x_j \partial x_j} + f_i, \tag{2}$$

with i and $j = 1, 2$ (cf. Figure 1). The variable P in equation (2) is the static pressure and f_i is the mean drag force of the canopy, defined as:

$$f_i = (f_x, f_y) = \left(-\frac{1}{2}C_d a \rho U^2, 0\right).$$

The coefficient a represents the frontal area of the vegetation per unit volume, i.e., the packing density of the elements (equal to 0.08 cm^{-1} in the experiments by *Ghisalberti and Nepf* [2004, 2005]), while C_d is the drag coefficient of the canopy. The mean flow is approximately parallel in the experiments, so that the equations reduce to:

$$\frac{\partial U}{\partial x}=0, \tag{3}$$

$$\frac{\partial U}{\partial t}=-\frac{1}{\rho}\frac{\partial P}{\partial x}+(\nu+\nu_t)\frac{\partial^2 U}{\partial y^2}-\frac{1}{2}C_d a U^2, \tag{4}$$

$$0=-\frac{1}{\rho}\frac{\partial P}{\partial y}. \tag{5}$$

In equation (4), we have assumed that the Reynolds stress can be modeled following Prandtl's mixing length model, with a constant mixing length l_m, as proposed by *Ghisalberti and Nepf* [2004]:

$$-\overline{u'v'}=\nu_t\frac{\partial U}{\partial y}=l_m^2\left(\frac{\partial U}{\partial y}\right)^2, \tag{6}$$

with ν_t the eddy viscosity. The streamwise pressure gradient depends on the surface slope $S=\sin\alpha_0$ of the channel bottom (which is slightly inclined in the experiments, with $0.18\times10^{-5}<S<10^{-4}$), so that in the case of steady-in-the-mean flow, equation (4) reads

$$\frac{\partial}{\partial y}\left[\left(\frac{\partial U}{\partial y}\right)^2\right]=\frac{1}{l_m^2}\left(\frac{1}{2}C_d a U^2-\nu\frac{\partial^2 U}{\partial y^2}-gS\right); \tag{7}$$

this equation can be solved numerically, for $0<y<y_2$. *Ghisalberti and Nepf* [2004] assume that $l_m=0.22\,(h-y_1)$ within the canopy ($y_1<y<h$) and $l_m=0.095\,t_{ml}$ in the portion of the shear layer above the canopy ($h<y<y_2$). The coefficients 0.22 and 0.095 arise from measurements and averaging over several experiments.

The drag coefficient C_d is deduced from the bulk drag coefficient C_{dA} of a random array of rigid cylinders. At large Reynolds numbers Re_d (based on the diameter d of a cylinder and U_1), this coefficient decreases with increasing cylinder density, $a\,d$, according to the best fit polynomial established by *Nepf* [1999]:

$$C_{dA}=\left(1+\frac{10}{Re_d^{2/3}}\right)[1.16-9.31ad+38.6(ad)^2-59.8(ad)^3], \qquad (ad<0.1) \tag{8}$$

with $C_d(y)=C_{dA}\eta(y)$ and $\eta(y)$ a function deduced experimentally by *Ghisalberti and Nepf* [2004]. Here, again, the profile of $\eta(y)$ is obtained via averaging over a large number of experimental runs. The vertical profile of the drag coefficient is displayed in Figure 2 for four cases taken from the papers by Ghisalberti and Nepf (cases G, H, J: *Ghisalberti and Nepf* [2004]; case I: *Ghisalberti and Nepf* [2005]).

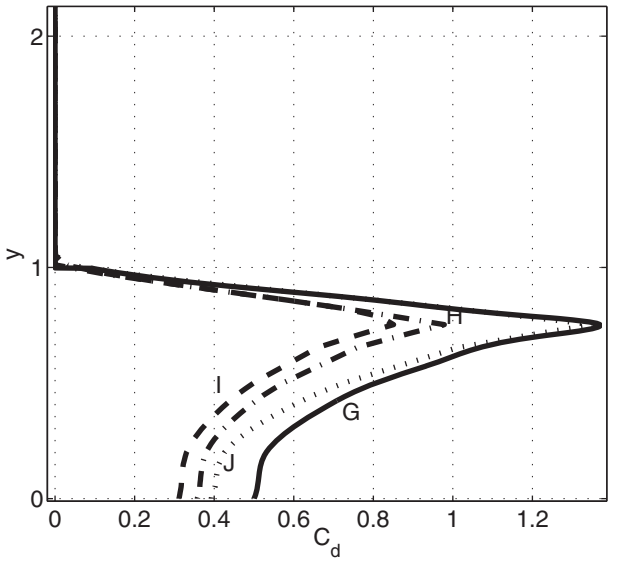

Figure 2. Vertical profile of the drag coefficient C_d for runs G, H, I, and J, along the vertical direction normalized with canopy height h.

The methodology used to compute U is based on a procedure initiated by *Ghisalberti and Nepf* [2004] and allows to automatically determine the value of the mean velocity at the top of the canopy, $U(h)$. It involves two independent relationships to be satisfied iteratively:

1. $h-y_1=\frac{1}{8.7\,C_d\,a}\left(\frac{(\Delta U)^2}{U(h)^2-U_1^2}\right)$, to evaluate the lower point of the mixing layer, y_1;
2. $\frac{\Delta U}{U(h)}\approx 16(a\,d)+1$ (for $0.016<ad<0.081$), to permit the evaluation of y_2.

The former equation stems from a balance between production and dissipation of shear-scale turbulent kinetic energy in a vegetated shear layer while the latter arises from the experimental correlation observed between $\Delta U/U(h)$ and the vegetation density in a range of values of $a\,d$

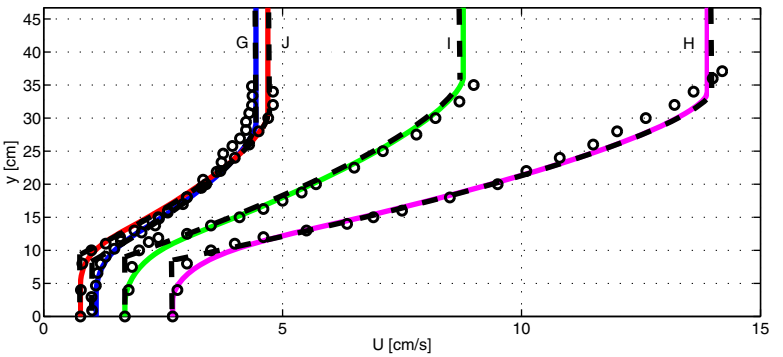

Figure 3. Mean velocity profiles of the flow through a rigid canopy, for various experimental runs (markers represent experimental data from *Ghisalberti and Nepf* [2004, 2005]). Solid and dashed lines are the mean flow profiles built using approach **A** and **B**, respectively. In physical units, it is $h=13.8$ cm and the free surface is at $y_\infty=46.7$ cm.

[*Ghisalberti and Nepf*, 2004, 2005]. The iterations yield, at convergence, velocity profiles in good agreement with measurements, as displayed in Figure 3.

In the second approach pursued here, the homogenized model of *Zampogna and Bottaro* [2016] is assumed to hold in the porous layer. In this zone, the streamwise velocity component satisfies the equation

$$U=\kappa_{11}\frac{gS}{\nu}. \tag{9}$$

Equation (9) is the dimensional Darcy's law, with κ_{11} the first component of the permeability tensor (cf. Appendix A), and U the Darcy's velocity (which can be significantly smaller than the actual pore speed, as function of the porosity of the medium). Even if equation (9) is linear, it is suitable to model high Reynolds numbers flow thanks to the fact that the permeability tensor, κ_{ij}, arises from the solution of a modified problem in which flow inertia is introduced via an Oseen approximation (and not from a canonical Stokes' problem) [*Zampogna and Bottaro*, 2016]. The permeability is thus an *apparent permeability*, not a function of the porous structure alone, but also of the flow (as shown in Table A1 in Appendix A).

Observing the sketch of the velocity profile in Figure 1, it seems reasonable to impose continuity of the streamwise velocity at a distance δ (*the penetration depth*) below the top of the canopy, to maintain some inertial effects right below the canopy's edge. The parameter δ plays the role of a fictitious interface position, as proposed by *le Bars and Worster* [2006]; equation (9) is thus applicable for $y\in[0,h-\delta]$. In the region above, the fictitious interface ($y\in[h-\delta,y_\infty]$), with y_∞ the coordinate of the free surface, the Reynolds-averaged steady solution (7), without canopy drag and neglecting the viscous term, yields a closed form for the mean streamwise speed:

$$U(y)=U(h-\delta)+\frac{2}{3}\frac{\sqrt{gS}}{l_m}\left[(y_\infty-h+\delta)^{\frac{3}{2}}-(y_\infty-y)^{\frac{3}{2}}\right]. \tag{10}$$

The condition at the fictitious interface is $U(h-\delta)=\kappa_{11}gS/\nu$. Also in approach **B,** the computed velocity distribution approximates well the measurements by Ghisalberti and Nepf (cf. Figure 3).

3. Instability Analysis: Neglecting Drag Within The Canopy

Neglecting the canopy drag corresponds to solving the inviscid stability equations within the flow domain to ascertain the effect of inflection points of the mean flow profile on the growth rate, frequency and wavelength of the most unstable mode. In the context of canopy flows, this approach has been initially advocated by *Raupach et al.* [1996] on the argument that the mixing-layer analogy provides an explanation for many of the observed distinctive features of canopy turbulence.

We scale velocity with the mean flow velocity U_m, length with the canopy height h, pressure with $\rho U_m{}^2$, and time with h/U_m, so that the dimensionless Rayleigh equation reads:

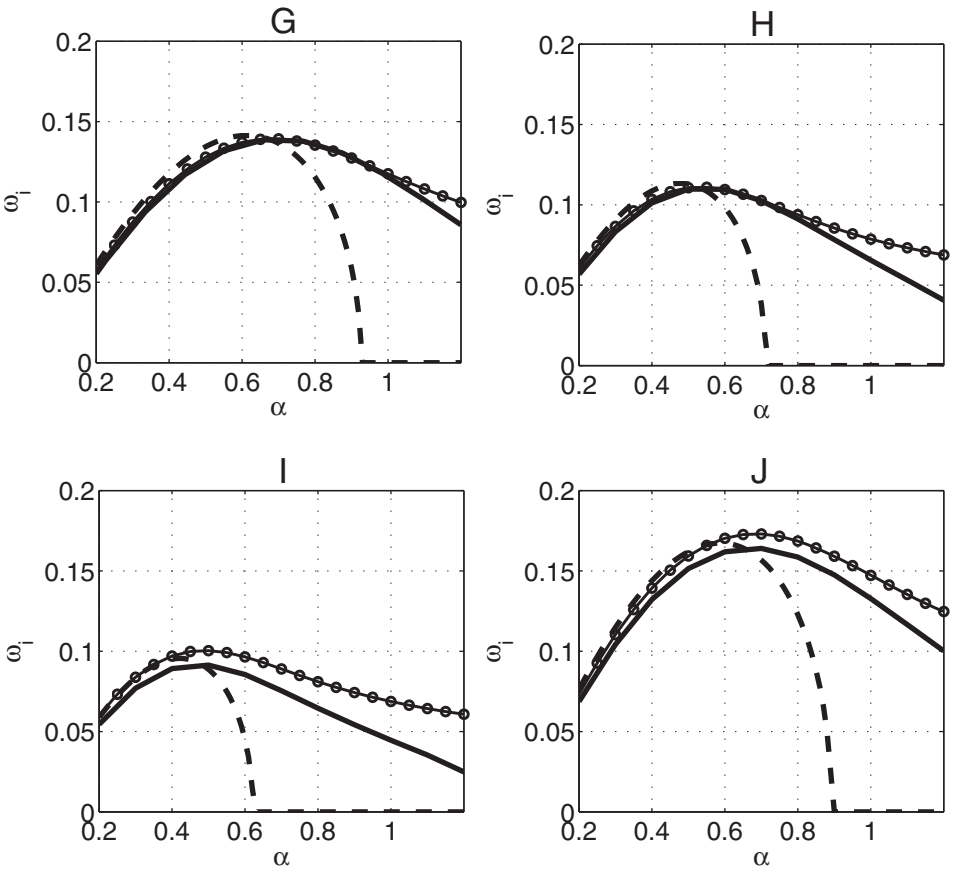

Figure 4. Temporal growth rate against wavenumber for the four cases, under Rayleigh's stability equation. Solid lines: numerical results (approach **B** with symbols); dashed lines: analytical results for piecewise-linear profiles.

$$\left[(U-c)(D^2-\alpha^2)-U''\right]v=0, \tag{11}$$

for the vertical velocity mode shape $v(y)$, with D and single prime denoting d/dy; disturbances are taken to behave like $e^{i\alpha x-i\omega t}$ and $c=\omega/\alpha$ is the phase velocity of the wave. The temporal stability problem studied here requires finding complex eigenvalues c for each assigned value of the (real) wavenumber α. The boundary conditions are simply $v=0$ at $y=0$ and y_∞ in approach **A** and y_∞ is here taken large enough for results not to be modified upon subsequent increments of y_∞.

For the case of approach **B,** a different condition must be imposed at the fictitious interface placed in $y=1-\delta$ where δ is here the dimensionless counterpart of the penetration depth introduced earlier. It will be precisely this condition which will force the occurrence of one unstable mode, considering that the profile of the mean velocity in the interval $[1-\delta, y_\infty]$ presents no inflection points (under **B**). At $y=1-\delta$ we impose, like we have done in the corresponding determination of the mean flow, continuity of pressure and of the vertical velocity component. We thus need the expression of p and v deep within the canopy, where U is constant. Solving equation (11) and imposing $v(0)=0$, we find that, for $y \leq 1-\delta$,

$$v_{canopy}=A\sinh(\alpha y), \quad p_{canopy}=-iA(U-c)\cosh(\alpha y), \tag{12}$$

so that, enforcing continuity of p and v at the fictitious interface, amounts to stating:

$$p(1-\delta)\tanh[\alpha(1-\delta)]+i(U-c)\,v(1-\delta)=0. \tag{13}$$

The results, in terms of temporal growth rate ω_i as function of α, are shown for the four cases G through J in Figure 4. The amplification factors of approaches **A** and **B** are in very good agreement with each other; variations can be ascribed to the mild differences between the two velocity distributions. A further confirmation of the results in Figure 4 is represented by the analytical solutions for the piecewise linear profiles in the semi-infinite domain $[0,\infty)$, the inclined piece of which is taken to be tangent to the numerical profile

of approach **A** at the point of maximum vorticity (cf. Figure 1). By enforcing continuity of the normal velocity and pressure at the point where the two linear profiles meet, it is found that:

$$\omega_i(\alpha)=\alpha\, Im\left(\pm\sqrt{-\left(\frac{U_2-U_1}{2}\right)^2+\frac{m}{2\alpha}(U_2-U_1)A-\frac{m^2}{16\alpha^2}B}\right), \tag{14}$$

with

$$A=\left(1-\frac{e^{-2\alpha y_1}+e^{-2\alpha y_2}}{2}\right), \tag{15}$$

$$B=\left(e^{-4\alpha y_1}+e^{-4\alpha y_2}-2e^{-2\alpha(y_2+y_1)}-4e^{-2\alpha t_{ml}}-4e^{-2\alpha y_1}+4e^{-2\alpha y_2}+4\right), \tag{16}$$

and $m=(U_2-U_1)/t_{ml}$ the slope of the profile at the inflection point. The three families of curves in Figure 4 are very close to one another at low to moderate values of α. The results indicate that the preferred wavenumber should be in the range $0.4 \leq \alpha \leq 0.7$ (which means that wavelengths go from about 9*h* to 16*h*).

To verify whether these values are reasonable, we turn to the detailed measurements and analysis of coherent eddies by *Raupach et al*. [1996]. Their results are for *honami* waves, i.e., for the oscillations of terrestrial canopies under the effect of wind, and thus apply to the case of a boundary layer (in their case the atmospheric boundary layer) which is much thicker than the vegetation height. Because of this fact, they are not directly applicable to the present case of aquatic canopies, but are nonetheless believed to provide relevant orders of magnitudes of the waves' characteristic features. The crucial parameter in the analysis by *Raupach et al*. [1996] is the *shear length scale* $L_s=U(h)/U'(h)$. L_s correlates well the streamwise spacing of the dominant canopy eddies; in particular, *Raupach et al*. [1996] state that

$$\alpha=\frac{2\pi h}{\gamma L_s}, \tag{17}$$

with $\gamma=8.1\pm0.3$, on the basis of observations from several experiments. We further note that L_s appears to be correlated also to the occurrence of *monami* waves in water: our analysis of the nine flow scenarios studied by *Ghisalberti and Nepf* [2002] suggests that *monami*s take place past a threshold value $L_s=0.65h$, and the corresponding instabilities display a wavenumber α which is always below 1.4. Further confirmation of the relevance of L_s for the case of coherent eddies over aquatic vegetation is provided by *Singh et al*. [2015].

Another result by Raupach and colleagues, based on two-point *u* correlations of *honami* waves in a sparse wheat canopy, is that the dominant circular frequency ω_r (the real part of $\omega=\omega_r+i\omega_i$) is approximated by

$$\omega_r=\frac{\pi}{\varepsilon}\frac{U(h)}{U_m}, \tag{18}$$

with $\varepsilon = 3 \pm 0.5$. A fit through the experimental data of *Ghisalberti and Nepf* [2002] for experiments in water provides a mean value of ε which is centered around 3.5.

A further correlation reported by *Raupach et al*. [1996] concerns the growth rate ω_i of the most unstable eddies, which is found to be proportional to $hU\prime(h)/U_m$.

Table 1 gives a summary of these predictions for the four experiments by Ghisalberti and Nepf analyzed here. On the basis of what stated above on L_s, we might expect scenarios G, H and I to lead to *monami* waves (and it is unexpected to find that case J apparently displays the largest instability growth rate).

Table 1. Significant Parameters of the Four Experiments Considered and Characteristic Wavenumber, Frequency, and Growth Rate of the Coherent Eddies Which Form Above the Canopy, According to Estimates by *Raupach et al*. [1996]

CASE	L_s/h	$U(h)(\mathrm{cms}^{-1})$	$U_m(\mathrm{cms}^{-1})$	$U\prime(h)(\mathrm{s}^{-1})$	α	ω_r	$hU'(h)/U_m$
G	0.73	2.22	2.75	0.22	1.06 ± 0.04	0.87 ± 0.14	1.104
H	0.73	5.95	8.29	0.59	1.06 ± 0.04	0.77 ± 0.13	0.982
I	0.76	3.60	5.24	0.35	1.02 ± 0.04	0.74 ± 0.12	0.922
J	0.55	1.88	2.73	0.25	1.42 ± 0.05	0.74 ± 0.12	1.835

It is immediately apparent from the table that the most unstable wavenumbers of the inviscid stability analysis are 100% off the experimental correlations. Also, the frequencies of the most unstable mode at the peak value of α are underestimated by the numerical results. These facts justify a closer look at the effect of the drag force exerted by the canopy on the flow.

4. Instability Analysis: Accounting for Canopy Drag

Drag is accounted for, in approach **A**, through a source term in the momentum equations, yielding a modified Rayleigh equation similar to that used by *Singh et al*. [2015] for the study of canopy flows. The difference from *Singh et al.*'s approach is that our drag coefficient C_d is not taken to be constant within the canopy but variable, as shown in Figure 2. Another difference lies in the fact that in the stability analysis we have considered a domain extending to a large value of y_∞, whereas they have limited the vertical extent of the domain to the actual size of the water channel of the experiments by *Ghisalberti and Nepf* [2002], enforcing at the free surface a no-shear condition. A final difference lies in the turbulence model used in *Singh et al*. [2015], based on a constant eddy viscosity through the canopy.

The equation used in approach **A** is:

$$(U-c)(D^2-\alpha^2)v-U''v-\frac{ia}{\alpha}D(C_dUDv)=0, \tag{19}$$

with $v=0$ at $y=0,y_\infty$.

Approach **B** couples Rayleigh's equation outside of the canopy to Darcy's equation within it, with a matching at the fictitious interface, $y=1-\delta$, on pressure and vertical velocity. Deep inside the porous zone, the dimensional disturbance equations are

$$\frac{\partial u_i}{\partial x_i}=0, \quad u_i=-\frac{\kappa_{ij}}{\mu}\frac{\partial p}{\partial x_j}. \tag{20}$$

Scaling the variables as in the previous section, the continuity equation remains unaltered and Darcy's equation becomes:

$$u_i=-\frac{\rho U_m h}{\mu}\frac{\kappa_{ij}}{h^2}\frac{\partial p}{\partial x_j}=-Re\,\mathcal{K}_{ij}\frac{d}{ah^2}\frac{\partial p}{\partial x_j}, \tag{21}$$

with $Re=\rho U_m h/\mu$ the Reynolds number and $d/ah^2=(l/h)^2$ a geometric coefficient related to the diameter ($d=0.64cm$) of the cylindrical fibers forming the canopy. From now on, for simplicity, we will indicate the group $Re\,\mathcal{K}_{22}\,d/ah^2$ with the symbol ξ.

Given the orthotropic nature of the canopy (cf. Appendix A), the off-diagonal terms of the permeability tensor $\mathcal{K}_{ij}$ vanish, and continuity yields

$$(D^2-\tilde{\alpha}^2)p=0, \tag{22}$$

with $\tilde{\alpha}=\alpha\sqrt{\mathcal{K}_{11}/\mathcal{K}_{22}}$. For the case of Stokes flow, it is $\mathcal{K}_{11}/\mathcal{K}_{22}=0.50$ (cf., *van der Westhuizen and du Plessis* [1996]), but here, on account of inertia, we have chosen to use $\mathcal{K}_{11}/\mathcal{K}_{22}=0.833$, as by computations from *Zampogna and Bottaro* [2016] at the present values of the Reynolds number (cf. Appendix Table A1). Upon application of the condition $v(0)=0$, it is found that p and v deep inside the canopy are given by:

$$p_{canopy}=\tilde{A}\cosh(\tilde{\alpha}y), \quad v_{canopy}=-\xi\tilde{\alpha}\tilde{A}\sinh(\tilde{\alpha}y). \tag{23}$$

Continuity of p and v at $y=1-\delta$ yields the boundary condition to be used when solving Rayleigh's equation in the domain $[1-\delta,y_\infty]$, i.e.,

$$v(1-\delta)+\xi\,\tilde{\alpha}\tanh[\tilde{\alpha}(1-\delta)]\,p(1-\delta)=0. \tag{24}$$

The other condition is simply $v|_{y_\infty}=0$.

Stability results are displayed as ω_i versus α in Figure 5. For approach **A,** the curves are very similar to those of the previous section, except for a damping effect experienced by the most unstable Kelvin-Helmholtz mode for all cases considered. This is precisely the effect predicted by *Py et al*. [2004] for the mixing layer instability over a flexible crop canopy. However, given that the wavenumber of largest growth seems still

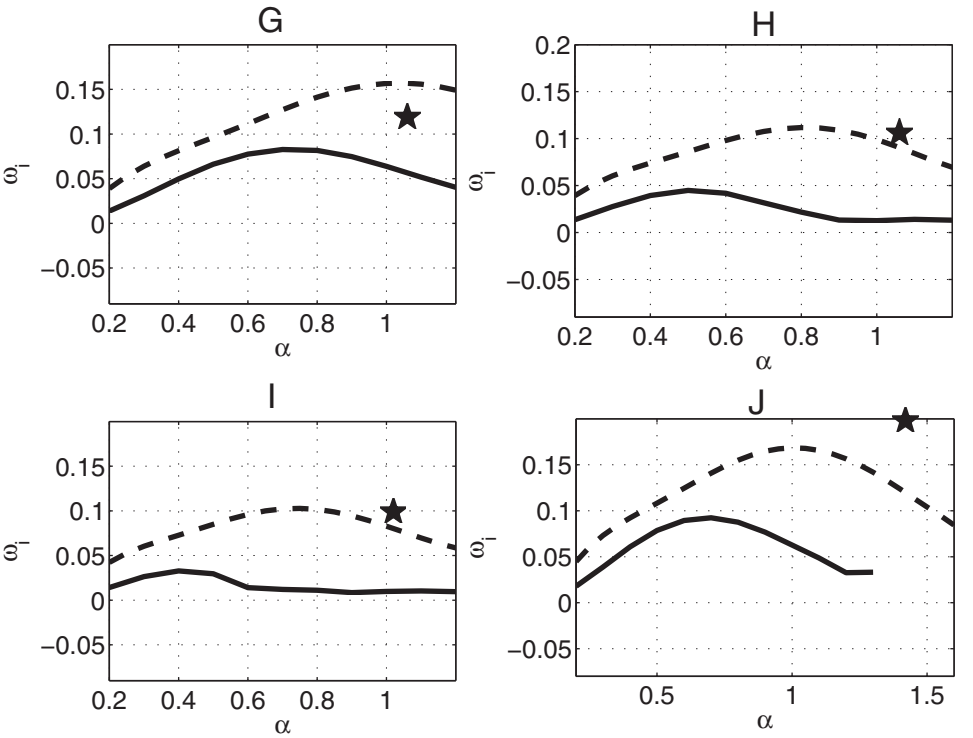

Figure 5. Stability curves for runs G, H, I, and J, accounting for drag. The solid and the dashed lines are based, respectively, on approach **A** and **B**. The stars indicate estimates of the most unstable mode, based on *Raupach et al.* [1996] correlations.

underestimated (at least against experimental correlations, cf. Table 1) something seems to be missing from model **A**. A similar argument motivated *Py et al.* [2004] to study a coupled fluid-structure model, accounting for the flexibility of the canopy via a wave equation [*Doaré et al.*, 2004]. Py and colleagues demonstrated that, for realistic values of the crop flexibility, the characteristics of the mixing layer instability were significantly modified, in particular with an increase of the most amplified wavenumber. This explained, at least in qualitative terms, discrepancies with measurements of the size of coherent eddies over a variety of canopies, as reported by *Finnigan* [2000].

In cases G through J examined here the canopy is not flexible, which means that it is the model itself (Rayleigh equation plus drag in the canopy, expressed with a drag coefficient C_d) which might have to be questioned. Model **B** proposed here represents an alternative, never explored before, which shows some promise. In fact, the results based on the coupled Rayleigh-Darcy system provide most unstable wavenumbers which approaches the heuristic predictions by *Raupach et al.* [1996], as shown in Table 2.

Also the growth rate of the most unstable mode is rather well correlated by the results of model **B** which indicate that

$$\frac{\omega_i U_m}{U'(h)h} = 0.108 \pm 0.014, \tag{25}$$

i.e., the ratio above is constant to within 13%. Conversely, the same ratio based on ω_i of approach **A** varies from 0.037 to 0.080.

Table 2. Most Unstable Modes for Approaches A and B, Accounting for Drag Throughout the Canopy

CASE	α_A	α_B	ω_{iA}	ω_{iB}	ω_{rA}	ω_{rB}
G	0.73	1.05	0.083	0.157	0.68	1.225
H	0.50	0.8	0.045	0.112	0.45	0.929
I	0.43	0.75	0.034	0.103	0.38	0.867
J	0.70	1.00	0.092	0.168	0.63	1.182

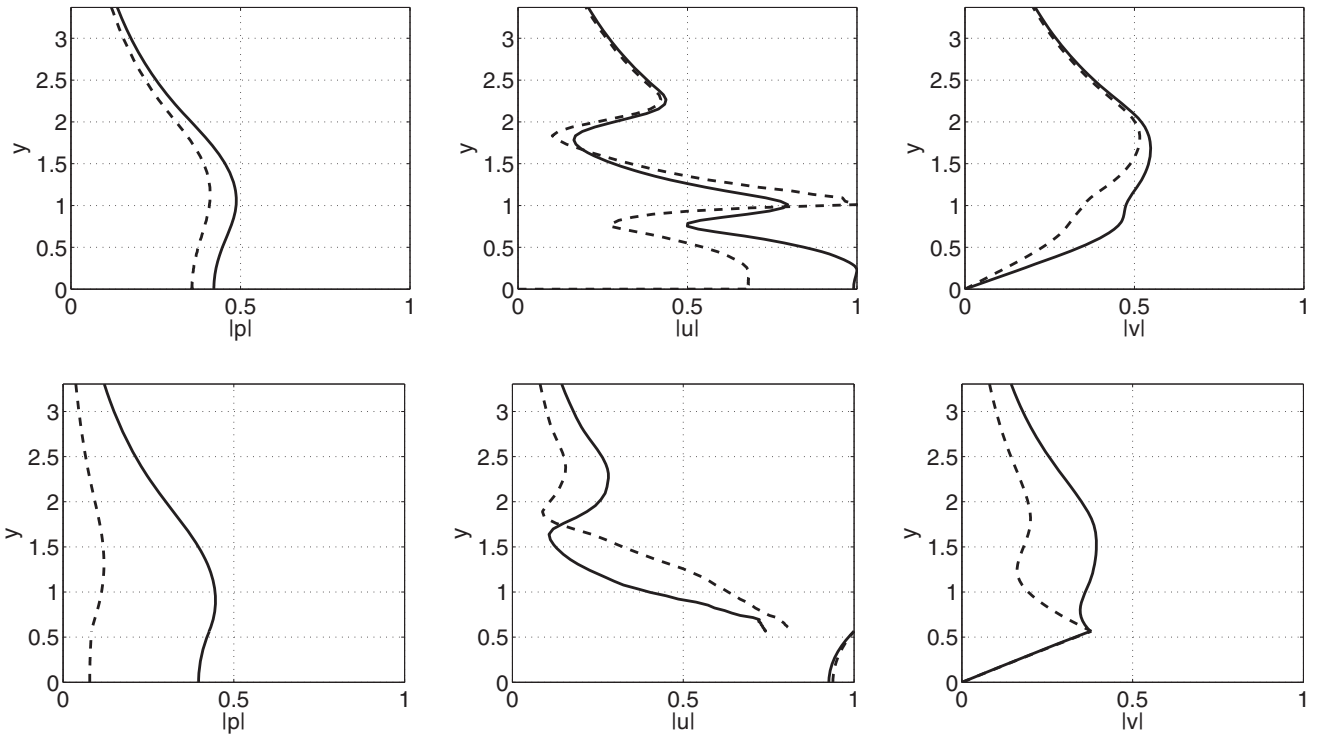

Figure 6. Modulus of the most unstable perturbation mode shapes for run G (α=0.7). Solid lines: Rayleigh equation. Dashed lines: including the drag force. Upper frames: approach **A**; lower frames: approach **B**.

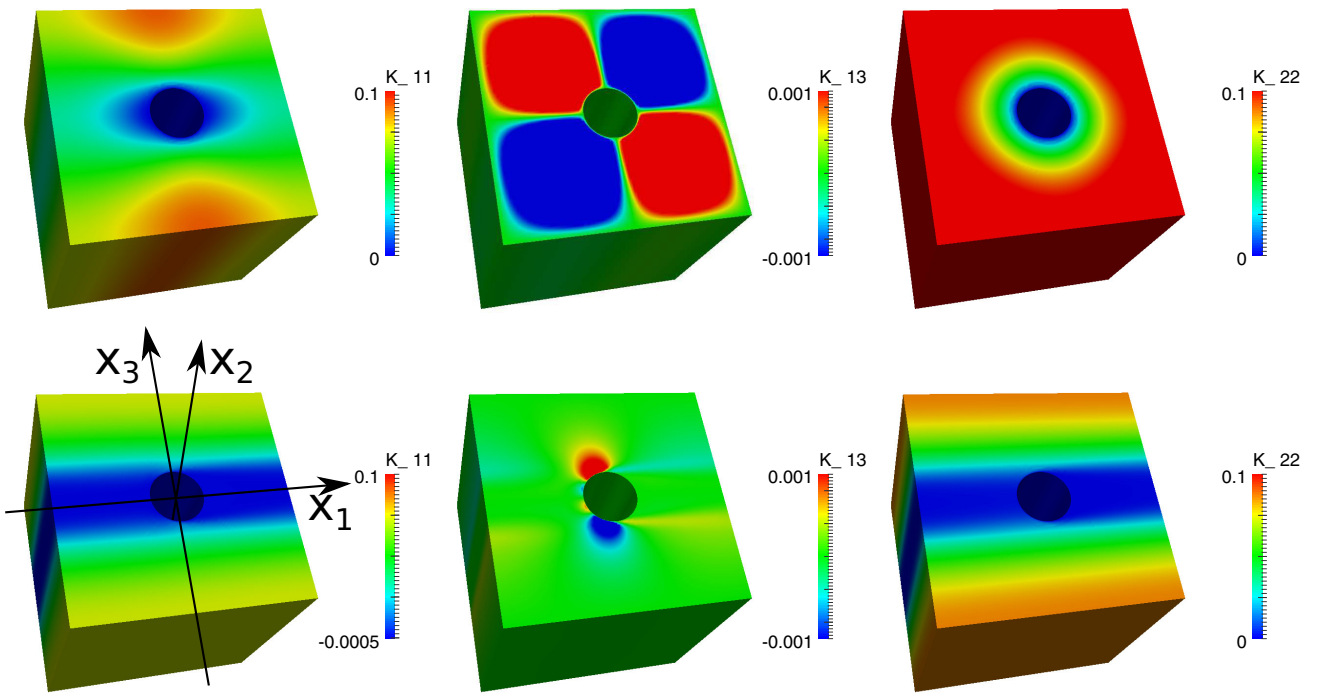

Figure 7. Microscopic solutions of equations (A3) in the elementary unit volume, for Stokes' flow (top row) and for inertial flow ($Re_l U_1^O$=764 with mean flow along x_1). The second configuration corresponds to case H of *Ghisalberti and Nepf* [2004]. Averaging K_{ij} over the unit cell we have K_{ij} (given in Table A1).

The most unstable circular frequencies ω_r of the analysis, on the other hand, exceed those of *Raupach et al.*'s correlation (cf. Table 2). On the basis of our results, the coefficient ϵ should be about half the value quoted in *Raupach et al*. [1996] for the case of *honami*.

An example of mode shapes is provided in Figure 6 for scenario G. For comparison purposes also the mode shapes of section 3 (no drag case) are reported; all cases refer to a wavenumber equal to 0.7. As for the curves of the growth rate, in the case without drag the eigenfunctions of the two approaches are similar. The main difference is in the fact that in approach **B** the horizontal disturbance velocity is not constrained to be continuous at the fictitious interface. Regarding the case with drag, instead, the main difference between the two approaches seems to be the nonsmoothness of the vertical velocity at $y=1-\delta$.

5. Conclusions

Shear layers generated by canopies are dominated by large-scale coherent vortex structures, initiated by Kelvin-Helmholtz instabilities [*Raupach et al*., 1996], known to be responsible for coherent, oscillatory motions of the vegetation, called *honami* or *monami*, whether in air or water.

The instability of these shear layers is studied here using two different approaches to model the flow, for the determination of the mean velocity profile (which fits in both cases the experimental data by *Ghisalberti and Nepf* [2004, 2005]) as well as to analyze the stability of the system. In terms of the mean flow, the Prandtl mixing length assumption appears to yield reasonable results in both approaches.

When we neglect the canopy drag, the two models display the same stability behaviors and yield similar results as the theoretical model based on a piecewise-linear mean profile, at least for the case of long waves. Comparisons of the most unstable modes with the measurements by *Raupach et al*. [1996] and *Ghisalberti and Nepf* [2004] suggest that drag within the canopy must be accounted for (a fact which had already been suggested by *Py et al*. [2004]).

We have thus tried to include the drag exerted by the canopy in two different manners. In the first instance, the drag force is a source term in the perturbation equations arising from the $-\frac{1}{2}C_d a U^2$ term in equation (4). This is the usual way of treating the drag within the canopy, with a single scalar coefficient C_d. The model by *Singh et al*. [2015] is based on this hypothesis; the difference between our approach and theirs is that we let C_d vary along the canopy as by experimental results.

In the second approach pursued, the (dense) canopy is treated as an anisotropic porous medium ruled by Darcy's law, with an *apparent* tensorial permeability $\mathcal{K}_{ij}$, function of the porosity of the medium and of the mean velocity of the fluid through the vegetation (which is here assumed undeformable). Thus, both the mean and the disturbance fields in the canopy can be expressed analytically (cf. equations (9) and (23)) and depend on the components of the *apparent* permeability tensor, on the Reynolds number *Re*, and on a geometric parameter characteristic of the vegetation bed. We believe that this second approach could partially answer one of the points raised by *Keylock* [2015] where the need for better models of dissipation in the near-bed region of fluvial flows is discussed, and considered necessary to address successfully river management and fluvial ecological issues.

The second approach yields reasonable estimates of the wavenumber α and of the frequency ω_r, at least when compared to existing correlations. The growth rate of the most unstable mode is proportional to the quantity $hU\prime(h)/U_m$, with almost the same constant of proportionality for the four configurations studied, in agreement with experiments by *Raupach et al*. [1996].

The study described here represents an attempt to model instabilities in canopy flows in a simple way, neglecting all those effects which are believed to be secondary. Approach **A** could possibly be improved by the inclusion of the near-wall boundary layer or by employing a turbulence model less diffusive than the simple eddy viscosity model to obtain the base flow in conditions not as idealized as in the present configuration [see, e.g., *Katul et al*., 2004; *Wilson and Shaw*, 1977]. Likewise, in approach **B** one could use Brinkman's equation to model viscous effects within the canopy or Forchheimer's equation to account for inertial terms. This second possibility could be employed to model the flow within the canopy, simulating a behavior which is closer to the real one, without any artificial parameter. In any case, only careful experimental measurements can justify the preference of a model over another and permit progress in the determination

of the most appropriate interface condition to be enforced at the boundary of a porous (or poroelastic) medium and a pure fluid region.

Appendix A: Homogenized Model

The homogenized model which allows to deduce equations (9) and (20) is briefly reviewed here. For more details, we refer to *Zampogna and Bottaro* [2016]. The starting point is the Navier-Stokes equations which hold in the regions of the canopy, sketched in Figure 1, occupied by the fluid phase. Assuming that the macroscopic pressure gradient is balanced by the microscopic diffusion term, the pressure scale $\mathcal{P}$ satisfies the order relation $\mathcal{P}/h=\mu V/l^2$ (with V the velocity scale within the canopy), so that

$$Re_l\left(\frac{\partial u_i}{\partial t}+u_j\frac{\partial u_i}{\partial x_j}\right)=-\frac{1}{\epsilon}\frac{\partial p}{\partial x_i}+\frac{\partial^2 u_i}{\partial x_j\partial x_j},\qquad \frac{\partial u_i}{\partial x_i}=0, \tag{A1}$$

where Re_l is the Reynolds number based on the microscale l and $\epsilon=l/h$ is a small parameter (with the present notations, the index 1 denotes the x axis, the index 2 is the y axis and 3 is z). The canopy is partitioned in microscopic elementary cubic cells of side l which include only one piece of a single cylindrical fiber (cf. Figure 7). The flow is assumed periodic inside this microscopic elementary volume. The homogenization procedure consists of two steps:

1. a multiple scale expansion on the basis of the parameter ϵ: the unknown fields are approximated at order 0 and the equations for the microscopic permeability, valid in the microscopic volume, for any given solid structure and porosity, are deduced;
2. an average over the small volume is defined and a macroscopic law for the flow is found.

The dimensionless governing equations obtained for the averaged flow (U, P) are

$$U_i=-\mathcal{K}_{ij}\frac{\partial P}{\partial x_j},\qquad \frac{\partial U_i}{\partial x_i}=0, \tag{A2}$$

where $\mathcal{K}_{ij}$ is the average value, over the microscopic cell, of the tensor K_{ij} which satisfies the following problem

$$-Re_l U_k^O\frac{\partial K_{ij}}{\partial x_k}=\frac{\partial A_j}{\partial x_i}-\delta_{ij}-\frac{\partial^2 K_{ij}}{\partial x_g^2},\qquad \frac{\partial K_{ij}}{\partial x_i}=0, \tag{A3}$$

where the vector A_j describes the dependence of the order ϵ pressure on the order 0 pressure gradient; it is not used since the fields are here approximated only up to order 0 [*Zampogna and Bottaro*, 2016]. The term $Re_l U_k^O\partial K_{ij}/\partial x_k$ comes from the Oseen approximation of the nonlinear term in (A1), and U_k^O is defined as

$$U_k^O=\frac{1}{V_{canopy}}\int_{V_{canopy}}U_k\,dV; \tag{A4}$$

V_{canopy} is the *total* volume of the macroscopic canopy region (solid plus fluid volume). Since in the Oseen approximation, there is an estimate of the macroscopic velocity field, in principle, an iterative procedure (over $Re_l U_k^O$) is needed to solve the equations for K_{ij} [*Zampogna and Bottaro*, 2016]. In the present case, there is no need to perform any iterative procedure because the values of $Re_l U_k^O$ are taken from the experiments by *Ghisalberti and Nepf* [2004, 2005]. Results for the permeability tensor K_{ij} are shown in Figure 7. The solid skeleton has an orthotropic structure, i.e., it has two planes of symmetry: it has been shown that, for this kind of structure, the permeability has a diagonal form and, in particular $\mathcal{K}_{11}=\mathcal{K}_{33}$. Conversely, the *apparent* permeability has a structure which depends on the flow intensity and direction. In the cases studied in this work, the flow is directed along $x=x_1$, so that only $Re_l U_1^O$ is different from zero. In this case, the symmetry of K_{ij} is lost only in one direction (cf. Figure 7) and $\mathcal{K}_{ij}$ is diagonal, with entries decreasing with the increase of the Reynolds number. The values of $\mathcal{K}_{ij}$ for two sample cases are

Table A1. Dimensionless Permeability for Fixed Porosity ($\vartheta=0.96$), in Case of Stokes Flow and for the Conditions of Case H[a]

	$\mathcal{K}_{11}$	$\mathcal{K}_{13}$	$\mathcal{K}_{22}$
$Re_l U_1^O=0$	$5.371\cdot10^{-2}$	0	$1.074\cdot10^{-1}$
$Re_l U_1^O=764$	$3.896\cdot10^{-2}$	0	$4.677\cdot10^{-2}$

[a]When inertia is present we have $\mathcal{K}_{11}/\mathcal{K}_{22}=0.833$.

shown in Table A1 (porosity $\vartheta=0.96$ and $Re_l U_1^O=764$ deduced by experiment H in *Ghisalberti and Nepf* [2004]).

Acknowledgments
The data used in this study are available from the authors upon request mailing to giuseppe.zampogna@edu.unige.it.

References

Battiato, I., and S. Rubol, (2014), Single-parameter model of vegetated aquatic flows, *Water Resour. Res.*, *50*, 6358–6369, doi:10.1002/2013WR015065.
Brevis, W., M. García-Villalba, and Y. Niño (2014), Experimental and large eddy simulation study of the flow developed by a sequence of lateral obstacles, *Environ. Fluid Mech.*, *14*, 873–893.
De Langre, E. (2008), Effect of wind on plants, *Annu. Rev. Fluid Mech.*, *40*, 141–168.
Doaré, O., B. Moulia, and E. De Langre (2004), Effect of plant interaction on wind-induced crop motion, *J. Biomech. Eng.*, *126*(2), 146–151.
Farquhar, T., J. Zhou, and H. Haslach (2003), A possible mechanism for sensing crop canopy ventilation, in *Sensors and Sensing in Biology and Engineering*, edited by F. Barth, J. Humprey, and T. Secomb, chap. 15, pp. 213–219, Springer, Wien.
Finnigan, J. J. (2000), Turbulence in plant canopies, *Annu. Rev. Fluid Mech.*, *32*, 519–571.
Ghisalberti, M., and H. M. Nepf (2002), Mixing layers and coherent structures in vegetated aquatic flows, *J. Geophys. Res.*, *107*(C2), doi:10.1029/2001JC000871.
Ghisalberti, M., and H. M. Nepf (2004), The limited growth of vegetated shear-layers, *Water Resour. Res.*, *40*, W07502, doi:10.1029/2003WR002776.
Ghisalberti, M., and H. M. Nepf (2005), Mass transport in vegetated shear flows, *Environ. Fluid Mech.*, *5*(6), 527–551.
le Bars, M., and M. G. Worster (2006), Interfacial conditions between a pure fluid and a porous medium: Implications for binary alloy solidification, *J. Fluid Mech.*, *550*,149–173.
le Bouteiller, C., and J. G. Venditti (2015), Sediment transport and shear stress partitioning in a vegetated flow, *Water Resour. Res.*, *51* 2901–2922, doi:10.1002/2014WR015825.
Katul, G. G., L. Mahrt, D. Poggi, and C. Sanz (2004), One- and two-equation models for canopy turbulence, *Boundary Layer Meteorol.*, *113*(1), 81–109.
Keylock, C. J (2015), Flow resistance in natural, turbulent channel flows: The need for a fluvial fluid mechanics, *Water Resour. Res.*, *51*, 4374–4390, doi:10.1002/2015WR016989.
Meroney, R. N. (1968), Characteristics of wind and turbulence in and above model forests, *J. Appl. Meteorol.*, *7*, 780–788.
Nepf, H. M. (1999), Drag, turbulence, and diffusion in flow through emergent vegetation, *Water Resour. Res.*, *35*(2), 479–489.
Novak, M. D., J. S. Warland, A. L. Orchansky, R. Ketler, and S. Green (2002), Wind tunnel and field measurements of turbulent flow in forests. Part I: Uniformly thinned stands, *Boundary Layer Meteorol.*, *95*(3), 457–495.
Py, C., E. De Langre, and B. Moulia (2004), The mixing layer instability of wind over a flexible crop canopy, *C. R. Mécaniq.*, *332*(8), 613–618.
Py, C., E. De Langre, and B. Moulia (2006), A frequency lock-in mechanism in the interaction between wind and crop canopies, *J. Fluid Mech.*, *568*, 425–449.
Raupach, M., J. J. Finnigan, and Y. Brunei (1996), Coherent eddies and turbulence in vegetation canopies: The mixing-layer analogy, *Boundary Layer Meteorol.*, *78*, 351–382.
Singh, R., M. M. Bandi, A. Mahadevan, and S. Mandre (2015), Linear stability analysis for monami in a submerged seagrass bed, *J. Fluid Mech.*, *786*(R1), 1–12.
van der Westhuizen, J., and J. P. du Plessis (1996), An attempt to quantify fibre bed permeability utilizing the phase average Navier-Stokes equation, *Comp. Part A*, *27*(4), 263–269.
Wilson, N. R., and R. H. Shaw (1977), A higher order closure model for canopy flow, *J. Appl. Meteorol.*, *16*(1), 1197–1205.
Zampogna, G. A., and A. Bottaro (2016), Fluid flow over and through rigid fibres, *J. Fluid Mech.*, *792*, 5–35.